Photophysics of blue light emitting polymeric mixed ionic-electronic conductors: Photoluminescence and absorption spectroscopy

G. Mauthner, H. Plank, and E. J. W. List*
Christian Doppler Laboratory Advanced Functional Materials, Institute of Solid State Physics, Graz University of Technology, A-8010 Graz, Austria and Institute of Nanostructured Materials and Photonics, Joanneum Research GmbH, A-8160 Weiz, Austria

F. P. Wenzl
Institute of Solid State Physics, Graz University of Technology, A-8010 Graz, Austria

M. Bouguettaya and J. R. Reynolds
The George and Josephine Butler Polymer Research Laboratory, Department of Chemistry, Center for Macromolecular Science and Engineering, University of Florida, Gainesville, Florida 32611, USA
(Received 22 May 2006; published 21 August 2006)

In this paper, the influence of the lithium salt lithium-trifluoromethanesulfonate (LiOTf) on the photophysics of three different oligo(ethylene-oxide) side-chain grafted poly(*p*-phenylene) (PPP) type polymers is studied by correlating polymer morphology to optical properties. It is shown that the introduction of the lithium salt leads to a phase transition from a lamellar-type ordered structure to a random amorphous phase, which is accompanied by an alteration of the optical properties of the polymers. Both the π-π^* as well as the triplet exciton (TE) absorption, exhibit a hypsochromic shift upon the addition of LiOTf. Moreover, a detailed study of the TE behavior of the polymer/LiOTf blend systems for different LiOTf concentrations was performed, including the generation rate of TEs from singlet excitons, the TE monomolecular decay, and the TE bimolecular annihilation process. One finds that upon increasing LiOTf concentration, both the TE generation rate and the TE lifetime increase, whereas the bimolecular annihilation process is diminished. These behaviors are correlated with the above mentioned order-disorder transition of the polymer system, which was confirmed by x-ray measurements.

DOI: 10.1103/PhysRevB.74.085208 PACS number(s): 78.20.−e, 78.30.Jw, 78.55.Kz, 78.66.−w

I. INTRODUCTION

Organic semiconductors, and in particular conjugated polymers, have attracted significant interest due to their potential applications in optoelectronics,[1–3] batteries,[4] for chemical sensing,[5,6] etc. Side chains render the polymers soluble in common organic solvents, which facilitates their processability by, e.g., spin coating, drop casting, or inkjet printing[7] of polymer solutions. A particular type of side chains, the oligo(ethylene-oxides) (OEO), offers another attractive property, which is ionic conductivity. Thus, conjugated polymers functionalized with OEO side chains are distinguished both by ionic and electronic conductivity [so-called polymeric mixed ionic-electronic conductors (pMIECs)],[8] which extends their potential applications from pristine solid state electrolytes[9] to utilizations in organic electronics, for example in light-emitting electrochemical cells (LEC).[10,11] Initial studies on LECs investigated blend systems of high molecular weight poly(ethylene oxide) (HMW-PEO) complexed with lithium-trifluoromethanesulfonate (lithium-triflate, LiOTf)—the prototype solid state electrolyte—and a luminescent conjugated polymer.[10,11] However, HMW-PEO reveals the disadvantage of crystallinity at room temperature, which on one hand lowers the ionic conductivity,[12] and on the other hand results in distinct phase separation between the hydrophilic ion conductor and the generally hydrophobic luminescent polymer that largely affects both the optoelectronic characteristics[13] and the reliability of the devices.[14] Therefore, the usage of OEO grafted conjugated polymers is a promising concept to overcome these difficulties, especially for applications where phase separation is a crucial issue.

In order to improve the performance of devices fabricated from a polymer or a blend consisting of a polymer and an alkali metal salt, as is necessary for LEC operation, it is essential to gain knowledge about the fundamental optical and electro-optical properties of the active layer. In particular, for organic light-emitting devices (light-emitting diodes from polymers as well as small molecules, LECs), the knowledge of the formation and decay pathways of the excited states created under device operation is essential; therefore, the analysis of the singlet exciton (SE) as well as the triplet exciton (TE) kinetics are main issues in order to enhance information of the electroluminescence behavior of the utilized organic materials and their blends with a salt.

As will be shown in the following for OEO grafted poly(*p*-phenylenes) (PPPs) and LiOTf as model systems, the SE and TE behavior significantly alters upon the addition of the salt. To do so, the properties of the excited species in the singlet [by means of π-π^* absorption and photoluminescence (PL)] and in the triplet manifold [by photoinduced absorption (PIA)] as a function of the LiOTf concentration were investigated.

When exciting a conjugated polymer by light, just SEs are formed; thus, TEs can only be created by intersystem crossing (ISC), which is allowed by spin-orbit coupling (SOC).

ISC from the singlet to the triplet manifold occurs mainly from the lowest excited singlet state S_1, since the internal conversion process is very fast. SOC between S_1 and the T_1 (the lowest excited triplet state) often vanishes and higher lying triplet states, which are energetically located in the vicinity of S_1, reveal high spin-orbit expectation values.[15] Quantum-chemical calculations of the ISC rates of oligo(phenylene ethynylene)s and oligothiophenes depicted that increasing the twist angle between adjacent rings enhances the ISC rates.[15] Such an enhancement of the twist angle between adjacent phenyl rings, thus disturbing the π-conjugation, may also be associated with an increased intrachain disorder, which can be artificially induced by blending the polymer with a salt.

The importance of triplet excitons is evident as they can be generated in organic light-emitting devices by two different ways, first, by recombination of a positive and negative polaron injected from the electrodes and secondly, via ISC of SEs from the singlet to the triplet manifold. Simple spin statistics predict that only 25% of the overall excitons generated in organic light-emitting devices are singlets, thus 75% do not contribute to the electroluminescence quantum yield (ELQY). In various studies performed in the past, it was suggested that SEs and TEs were generated with different cross sections,[16] which had been also confirmed by quantum-chemical calculations,[17] and ELQYs up to approximately 50% were reported. However, recently, experiments have shown that the ELQY of organic light-emitting devices is restricted to the spin statistics meaning that only a 25% singlet yield can be obtained.[18]

In the following studies, OEO grafted PPPs, which were successfully applied in light-emitting diodes[19,20] and LECs,[19] are depicted to shed some more light on the singlet and triplet kinetics of optoelectronic devices utilizing pMIECs.

II. EXPERIMENTAL METHODS

The oligo(ethylene-oxide) grafted PPP-type polymers PPP-OR11, PPP-R10, and PPP-R10/OR11 were prepared using Suzuki polymerization methods as previously reported.[21] The two homopolymers PPP-OR11 and PPP-R10, the copolymer PPP-R10/OR11—which is a random composition of the two homopolymers—and the lithium salt LiOTf were dissolved in oxygen-free tetrahyrdofuran (THF) and stirred for 12 h under an argon atmosphere. Films of the pristine polymers and polymer/LiOTf blend systems were fabricated in an argon glove box by spin casting 12 mg/ml solutions (ratio polymer to LiOTf 20:4, 20:6, 20:8, and 20:16 by weight), yielding films of approximately 100 nm thickness on quartz substrates. Diluted solutions of the pristine polymers and polymer/LiOTf blends with polymer concentrations in the range of μg per ml solvent were prepared in order to investigate the photophysical properties of the polymer in solution, avoiding any self-absorption effects. Ultraviolet/visible (UV/Vis) absorption and PL spectra were recorded with a Perkin-Elmer Lambda 9 spectrophotometer and a Shimadzu RF5301 spectrofluorimeter, respectively. Samples for the PIA measurements were mounted within an optical cryostat (temperature of about 77 K) under dynamic vacuum (pressure less than 10^{-5} mbar to prevent photooxidation). The pump beam was provided by an argon ion laser in multiline UV mode (351 nm and 364 nm). This excitation beam was modulated by a chopper at a frequency of 17 Hz, providing the reference for the lock-in amplifier. A tungsten halogen lamp provided the light for the absorption measurements. All PIA spectra were corrected for the PL and optical throughput of the setup. X-ray measurements were performed with a Siemens D501 Krystalloflex powder diffractometer (coupled theta/2theta).

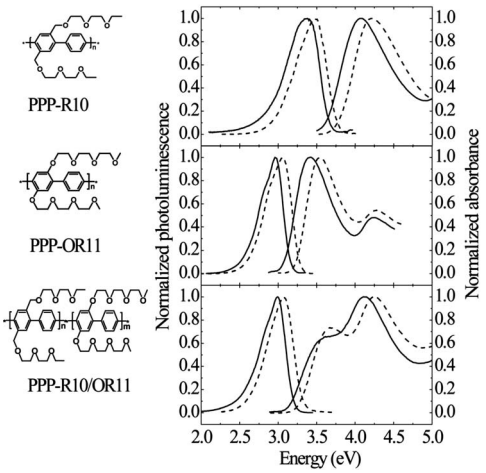

FIG. 1. Chemical structures of the three investigated PPP-type polymers: PPP-R10 (left top), PPP-OR11 (left middle), and the copolymer PPP-R10/OR11 (left bottom). Right side: Absorbance and PL spectra of diluted solutions (dashed line) and spin-cast films (solid line) of the polymers.

III. RESULTS AND DISCUSSION

The three conjugated polymers investigated in this study are OEO side-chain grafted poly(*p*-phenylene)s (the chemical structures are depicted in Fig. 1); of these, two are homopolymers—a bis-(alkyl)-substituted PPP, abbreviated as PPP-R10, and a bis-(alkoxy)-substituted PPP, abbreviated as PPP-OR11—and the third is a copolymer abbreviated as PPP-R10/OR11.[21] The copolymer consists of a random composition of segments of the two homopolymers. From NMR studies, it is estimated that the copolymer consists of approximately 51% PPP-OR11 and 49% PPP-R10 segments. PPP-R10 and PPP-OR11 differ by the specific composition of the OEO side chains: For PPP-R10 they are grafted by carbon atoms, which, in the case of PPP-OR11, are replaced by oxygen atoms, so that the side chains of PPP-OR11 contain one more oxygen atom. The resulting consequences on the photophysical properties will be discussed in detail below.

A. Photoluminescence and π-π^* absorption of the pristine polymers

Figure 1 shows the absorption and the PL spectra of diluted solutions and thin spin-coated films of PPP-R10, PPP-OR11, and PPP-R10/OR11. When analyzing the absorption

and the emission spectra of the three PPP-type polymers, it is evident that the spectra possess no vibrational structure. This absence of a well-resolved vibronic structure in the absorption and the emission is indicative for the presence of different conjugation lengths, resulting in a distribution of energetic sites. Additionally, since the phenyl rings of the PPPs are capable of twisting around the axis defined by the polymer backbone, a distinct geometry change during the transition from the ground state to the excited state (documented by rather differently shaped ground and excited state energy parabolas) is sustained.[22] As a consequence of this interring tilt angle alteration between the two conformations, the ring torsional mode strongly couples to the optical transition. Similar experimental results were found for biphenyl[23] and *p*-terphenyl.[22]

Analyzing the solid state spectra of the polymers, the maxima of the absorption peak of PPP-R10 and PPP-OR11 are found at 4.08 eV and 3.43 eV, respectively. The PL maxima of PPP-R10 and PPP-OR11 are located at 3.38 eV and 2.96 eV, respectively. Both the absorption and the PL spectra of PPP-OR11 reveal a distinct redshift in comparison to those of PPP-R10, which is a consequence of the different side-chain types. Since the side chains of PPP-OR11 are grafted by oxygen atoms, the redshift is caused by two effects: The oxygen atoms (a) donate electron density from the π-electron system raising the HOMO level of the backbone[24] and (b) have less steric interaction with the hydrogen atoms of the adjacent phenyl rings than the methylene groups, which results in a more planar structure of the backbone. While (a) generally leads to an overall reduction of the optical gap (confirmed by quantum-chemical calculations), (b) seems to promote this effect: the more planar conformation of the backbone gives rise to minor disturbance of the π-electron system and therefore to a lower band gap compared to PPP-R10.

A further remarkable feature distinguishing the homopolymers is the large difference of the Stokes shifts. For PPP-R10 the Stokes shift is 0.75 eV while that of PPP-OR11 is only 0.49 eV. This energy difference of 0.26 eV arises from different degrees of conformational changes between the ground and the excited states of the two polymers. The particular torsional angles of adjacent phenyl rings largely differ for the two polymers in the ground state, which results in the considerable energy difference of the absorption maxima (0.65 eV). However, in the excited state the π-electron system is altered, which leads to a modification of the geometric structure. The backbones of both polymers become more planar, the difference of the twist angles decreases, and consequently the difference of the PL peak maxima of PPP-OR11 and PPP-R10 exhibits only 0.42 eV compared to the 0.65 eV in the instance of the π-π^* absorption.

As already mentioned before, the copolymer PPP-R10/OR11 consists of segments of both homopolymers. Theoretical work on other copolymers comprising low and high band-gap segments suggests that the band gap is the weighted average of the gap values of the segments of the homopolymers.[25] However, the solid state absorption spectrum of PPP-R10/OR11 does not show features that can be attributed to such "weighted average" but clearly displays contributions of the PPP-R10 and PPP-OR11 segments. The characteristic shoulder in the absorption spectrum at approximately 3.52 eV has nearly the same energetic position as the maximum of the PPP-OR11 absorption. The main absorption peak at 4.12 eV originates from the PPP-R10 segments. The solid state PL spectra of the copolymer and PPP-OR11 exactly match, which can be ascribed to Förster energy transfer or to intra—or interchain exciton migration[26] after photoexcitation from the higher energetic PPP-R10 to the lower energetic PPP-OR11 segments, which subsequently act as emission centers.

TABLE I. PL and π-π^* absorption maxima of the three investigated polymers in solution and of spin-cast films.

	PL maximum (eV)		π-π^* absorption maximum (eV)	
	Solution	Film	Solution	Film
PPP-R10	3.47	3.38	4.22	4.08
PPP-OR11	3.05	2.96	3.54	3.43
PPP-R10/OR11	3.08	3.00	4.26	4.12

In principle the spectra of the polymers in diluted solution reveal the same shape as the film spectra, however, in case of the solution spectra the maxima of the PL and the π-π^* absorption are shifted by about 0.1 eV to higher energies (see also Table I).

The observation of a bathochromic shift in the absorption and the emission characteristics leads to the conclusion that the PPP backbones are flattened into a more tight, planarized conformation in the solid state by an ordering effect (solid state stacking). No evidence for distinct interchain interactions of the π-electron systems was observed (ground state aggregate or excimer formation).

B. Photoluminescence and π-π^* absorption of the polymers blended with LiOTf

In order to study the influence of an alkali metal salt on the photophysical properties, in Fig. 2 the solid state π-π^* absorption and the PL spectra of the three pristine polymers PPP-R10, PPP-OR11, and PPP-R10/OR11 are compared with the corresponding polymer/LiOTf blends. The ratio of polymer to LiOTf of each blend was 20:4 by weight, a value typically used for the fabrication of LECs.

When comparing the spectra of the pristine and the salt-blended films, a small hypsochromic shift is observed for both the absorption and the PL, an effect which is caused by the presence of the ionic species. The accompanying disorder results in an alteration of the conformation and/or the electron density of the polymer backbones. This effect is termed an ionochromic effect;[5,27] thus, the exact values for the optical band gaps of the polymers depend on the presence and the amount of the ionic species. The ionochromic effect is also known for other conjugated polymers containing of OEO side chains, such as poly[2,5-bis(triethoxy-methoxy)-1,4-phenylene vinylene] (BTEM-PPV).[6,28] Table II summa-

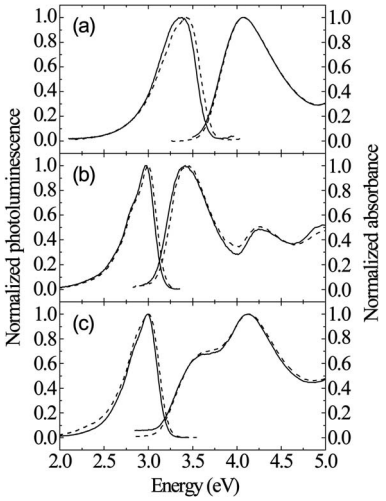

FIG. 2. Absorbance and PL film spectra of PPP-R10 (a), PPP-OR11 (b), and PPP-R10/OR11 (c) in its pristine (solid line) and LiOTf blended (dashed line) states (polymer to salt 20:4 by weight).

rizes the π-π^* absorption and the PL peak maxima for the pristine and the LiOTf blended systems.

In order to analyze the alteration of the photophysical properties of the singlet and the triplet excitons with increasing salt concentration, the system PPP-R10/LiOTf will be representatively discussed in the following. Figure 3 depicts the π-π^* absorption of PPP-R10 films in the pristine and the salt-blended states for different concentrations of LiOTf (ratios 20:4, 20:6, 20:8, and 20:16 by weight). The absorption spectra reveals two distinct trends with increasing salt concentration: first, a hypsochromic shift of the peak maxima and secondly, a broadening of the peaks. The absorption maxima shift from 4.09 eV for pristine PPP-R10 to 4.26 eV for PPP-R10:LiOTf 20:16 by weight. This blueshift, as well as the broadening of the spectra, indicates that the addition of LiOTf induces disorder in the system, which increases the twist angle between neighboring phenyl rings of the PPP backbone and hence diminishes the π-conjugation. The peak broadening can be explained by the fact that some of the segments still do not form complexes with lithium ions. By

TABLE II. π-π^* absorption and PL maxima of the three investigated polymers in the pristine and LiOTf blended solid states (polymer:LiOTf=20:4 by weight.)

	Absorbance max. (eV)	PL max. (eV)
PPP-R10	4.09	3.38
PPP-R10+ LiOTf	4.10	3.41
PPP-OR11	3.43	2.96
PPP-R10+ LiOTf	3.44	3.00
PPP-R10/OR11	4.12	2.995
PPP-R10/OR11+ LiOTf	4.15	3.002

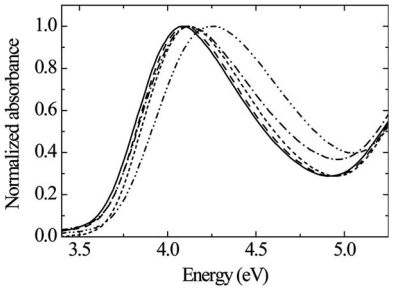

FIG. 3. π-π^* absorption spectra of PPP-R10 as a function of the LiOTf concentration. (Solid line) pristine PPP-R10. The ratios polymer to LiOTf are 20:4 (dashed line), 20:6 (dashed-dotted line), 20:8 (short dashed line), and 20:16 (dashed-dotted-dotted line) by weight.

means of infrared[29] and Raman studies,[30] it was found that ion pairs dominate in OEO grafted conjugated polymer/LiOTf blend systems, because of the low dielectric constant of the OEOs. The low degree of ion dissociation lets one conclude that the lower energetic part of the absorption spectrum stems from "undisturbed" noncomplexed polymer segments, and the higher energetic part from "disturbed" complexed ones and additionally from segments that are sterically disturbed by ion pairs and/or aggregates.

C. X-ray diffraction and disorder

In order to confirm the wavelength shift and the broadening of the absorption peak of PPP-R10/LiOTf blends with increasing salt concentration, which is assumed to be a result of disorder, morphological investigations on the blend systems have been performed. Lauter *et al.*[31] proposed an idealized structural model for OEO grafted PPP type polymers. Within this model, a lamellar order constituted by PPP layers separated by the side chains was predicted for the polymer in its pristine state. In order to study the influence of LiOTf on this order, x-ray measurements at room temperature were performed.

Figure 4 illustrates the x-ray diffractograms of drop-cast films of pristine PPP-R10 and PPP-R10 blended with LiOTf (ratio PPP-R10:LiOTf=20:4 by weight). The diffractogram

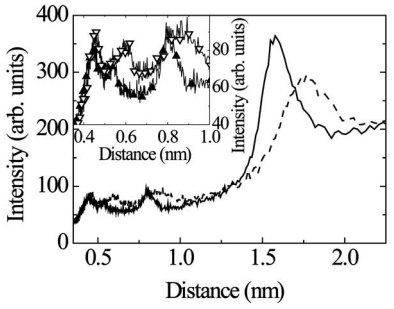

FIG. 4. X-ray diffractograms of drop-cast films of pristine PPP-R10 (solid line) and PPP-R10 blended with LiOTf (PPP-R10:LiOTf=20:4 by weight) (dashed line). Inset: Second and third order of the main peaks; (filled triangles) pristine PPP-R10, (open triangles) PPP-R10:LiOTf=20:4 by weight.

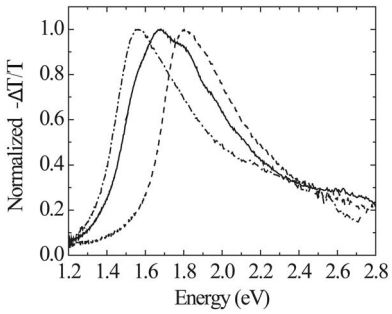

FIG. 5. PIA spectra of the pristine PPP-type polymers. (dashed line) PPP-R10, (dashed-dotted line) PPP-OR11, and (solid line) PPP-R10/OR11.

of the pristine drop-cast polymer film depicts a sharp peak at 1.58 nm, which can be related to the distance between the main chain layers in the polymer film. This reflection indicates lamellar ordering of the hydrophobic polymer backbones in the film, which are separated by the hydrophilic OEO side-chain matrix. At 0.8 nm and 0.53 nm, the second and third order of this peak can be observed. However, additional contributions, e.g., from interchain spacing, complicate a comprehensive interpretation.

Comparing the peak positions and their heights, the consequences of salt addition on the lamellar order becomes evident. On the one hand, the peak undergoes a distinct shift in accordance with a higher interchain distance (from 1.58 nm in the pristine state to approximately 1.77 nm in case of the 20:4 blend). Accordingly, also the maxima of the higher orders shift in the same direction, which is displayed in the inset of Fig. 4. Simultaneously, the peak height decreases upon addition of the lithium salt. The former characteristic is due to an ion-induced enhancement of the PPP-layers spacing, while the latter one points to disorder as a consequence of the addition of the lithium salt, indicating that the lamellar order is reduced.

D. Photoinduced absorption of the pristine polymers

To study the nature of the nonemissive excited entities (TEs and polarons) of PPP-R10, PPP-OR11, and PPP-R10/OR11 in their pristine and LiOTf complexed states, PIA measurements were performed. Since the TE properties are strongly affected by the amount of order, the experiments in this section aim to address the influence of the TE properties on the LiOTf concentration. Figure 5 shows the PIA spectra and TE absorption features ($T_1 \rightarrow T_n$), respectively, of the pristine PPP-type polymers under investigation.

The location of the TE features of the polymers was confirmed by quantum-mechanical calculations.[32] Comparing the spectra of the homopolymers (PPP-OR11 and PPP-R10), it is evident that the $T_1 \rightarrow T_n$ transition maximum of PPP-OR11 reveals a distinct redshift. PPP-OR11 exhibits its maximum at 1.54 eV, whereas that of PPP-R10 is located at 1.80 eV. This bathochromic shift indicates that the different side chains, as in the case of the above-discussed π-π^* absorption spectra, cause a more extended π-electron system in the case of PPP-OR11 and thus a lower $T_1 \rightarrow T_n$ transition

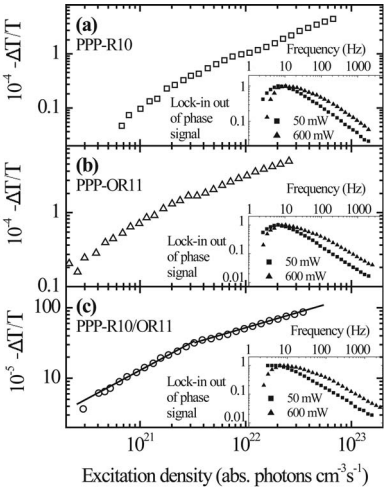

FIG. 6. Dependence of the PIA signal of pristine PPP-R10 (a), PPP-OR11 (b), and PPP-R10/OR11 (c) on the laser intensity. Inset: Out-of-phase signal of the lock-in amplifier in the monomolecular and the bimolecular TE decay regime depending on the modulation frequency.

energy. This is confirmed comparing the PIA spectra of PPP-OR11 and PPP-R10 with PIA spectra of other PPP-type polymers, such as poly(9,9-dioctylfluorene) (PFO)[33] and methyl substituted ladder-type poly(*p*-phenylene) (m-LPPP),[34] which possess planarized conjugated backbones due to bridges between adjacent phenyl rings. The maxima of the $T_1 \rightarrow T_n$ transition energies of PFO and m-LPPP were found at 1.4 eV and 1.3 eV, respectively, which is lower than the maxima of the two homopolymers investigated.

The copolymer, which is a composition of PPP-OR11 and PPP-R10 segments, shows the TE absorption contributions of both homopolymers. This is evidenced by shoulders at the positions of the PPP-R10 and PPP-OR11 triplet absorption maxima. The triplet absorption maximum is located at 1.67 eV and therefore lies exactly in the middle between that of the PPP-R10 and PPP-OR11. The signal of the other nonemissive entity of the polymers, the polarons, is obviously too weak for studies.

One has to point out that the TEs of the copolymer PPP-R10/OR11 reveal different behavior (PIA spectrum) compared to its SEs (π-π^* absorption). The singlets migrate from the PPP-R10 to the lower energetic PPP-OR11 segments, which subsequently serve as recombination centers (Fig. 2), whereas the TEs can be detected on the PPP-OR11 as well as on the higher energetic PPP-R10 segments. These discrepancies can be explained by the different timescales of the triplet absorption (approximately 10^{-15} s) and the energy transfer process between the different segments of a copolymer (approximately 10^{-12} s). In other words, the TEs of the PPP-R10 segment are excited to the T_n states before they can relax to the lower energetic PPP-OR11 segments.

In principle one can quantify the monomolecular lifetime $\tau_{\mathrm{TE,mono}}$ and the ISC conversion rate of the SE to the TE (TE quantum yield $\eta_{\mathrm{SE}\rightarrow\mathrm{TE}}$) at low excitation densities (monomolecular decay range) as well as the equivalent bimolecular lifetime $\tau_{\mathrm{TE,bi}}$ and the bimolecular annihilation parameter γ_{TE} at high excitation densities (bimolecular decay regime).[35]

TABLE III. Monomolecular TE lifetime τ_{TE}, TE quantum yield $\eta_{SE\rightarrow TE}$, and bimolecular annihilation parameter γ_{TE} of PPP-R10, PPP-OR11, and PPP-R10/OR11.

	PPP-R10	PPP-OR11	PPP-R10/OR11
τ_{TE} (ms)	21	25	25
$\eta_{SE\rightarrow TE}$ (-)	8E−4	3E−4	8E−4
γ_{TE} (cm^{-3} s^{-1})	4E−16	7E−16	3E−16

Figure 6 shows intensity-dependent TE absorption measurements of PPP-R10, PPP-OR11, and PPP-R10/OR11 films recorded at the $T_1 \rightarrow T_n$ absorption maximum [obtained by the conventional PIA measurements (Fig. 5)]. Comparing the amount of TEs as a function of the laser excitation intensity for the different polymers, the transition from the monomolecular to the bimolecular decay regime can be clearly observed as a change of the curves' slope (sketched for PPP-R10/OR11). The insets of Fig. 6 show the dependence of the out-of phase signal of the lock-in amplifier on the chopper frequency measured in the monomolecular and bimolecular TE decay regimes. A detailed description of the $\tau_{TE,mono}$, $\eta_{SE\rightarrow TE}$, and γ_{TE} calculation is given in the appendix, while the determined values are displayed in Table III.

The values of $\tau_{TE,mono}$ are similar for all three polymers investigated and are in the range of 25 ms. Comparing these values with the monomolecular TE lifetime of polymers with more planar backbones (for m-LPPP this value was found to be about 10 ms),[35,36] it can be concluded that the less twisted and distorted the polymer backbone, the lower the TE lifetimes. This is attributed to defects, which act as TE quenching centers and can be more easily reached in a well-developed π-electron system.

The TE quantum yield $\eta_{SE\rightarrow TE}$ of all three polymers is in the range of 10^{-4} and 10^{-5}, while the bimolecular annihilation parameter of triplet excitons γ_{TE} is in the range of 10^{-15} to 10^{-16} cm^3 s^{-1}. The yields $\eta_{SE\rightarrow TE}$ are similar to those observed for other conjugated polymers, e.g., m-LPPP.[37] One reason why $\eta_{SE\rightarrow TE}$ of PPP-R10 is somewhat higher than observed for PPP-OR11 can be assigned to the larger twisting angle between adjacent phenylene rings, which increases the energetic disorder. This is favorable for the formation of polarons and hence triplet excitons formed therefrom. The bimolecular annihilation parameter is related to the diffusion coefficient of the TEs by Eq. (A3) (see Appendix). A calculation of the diffusion coefficients D_{TE} for all three polymers yields $D_{TE} \sim 10^{-10}$ cm^2 s^{-1}, which is in good agreement with other organic materials.[23]

E. PIA measurements of LiOTf blended polymer films and TE kinetics

Modification of the polymer system by the addition of LiOTf alters the structural order of the polymer chains (see Fig. 4). In the following, the variations of the TE properties (changes of TE generation rate and their kinetics) upon the addition of LiOTf are discussed.

Figure 7 depicts the TE absorption features of PPP-R10, PPP-OR11, and PPP-R10/OR11 in their pristine and LiOTf blended states (polymer to LiOTf 20:4 by weight). In each instance the TE absorption spectra of the LiOTf complexed films display a shift to higher energies and a peak broadening compared with their pristine state, consistent with the observations obtained for the π-π^* absorption. These hypsochromic shifts provide additional evidence for a reduced π-conjugation of the backbones induced by the alkali metal salt added and the related increase of disorder.[38]

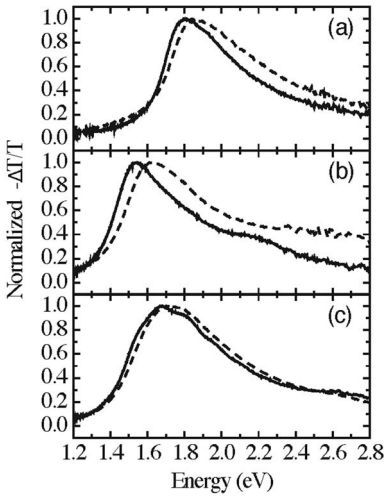

FIG. 7. TE absorption features of PPP-R10 (a), PPP-OR11 (b), and PPP-R10/OR11 (c) in their pristine (solid line) and LiOTf blended (dashed line) states (polymer:LiOTf=20:4 by weight).

In order to analyze the influence of LiOTf addition on the TE kinetics in detail, intensity-dependent PIA measurements (varying the excitation intensity of the laser and density of absorbed photons N_{abs}, respectively) and frequency-resolved PIA measurements (varying the frequency at constant excitation intensity) were performed. Since both trends—the blueshift of the peak maxima and peak broadening with increasing salt concentration—are equal for all the polymers investigated, PPP-R10/LiOTf blends were chosen as a representative system. PIA measurements were performed of pristine PPP-R10 and PPP-R10/LiOTf blends (20:4, 20:6, 20:8, and 20:16 by weight). Figure 8 shows the PIA spectra of these five samples.

With increasing salt concentration the $T_1 \rightarrow T_n$ absorption maximum shifts from 1.80 eV (pristine PPP-R10) to 1.99 eV (PPP-R10 blended with LiOTf 20:16 by weight). The full width at half maximum (FWHM) of the TE absorption peak increases from 0.508 eV to 0.919 eV. Both characteristics can be ascribed to a reduction of the π-conjugation of the polymer backbones as a consequence of the addition of ionic species and the resulting increase of disorder, as also observed for the π^*-π absorption of the systems (see Fig. 3).

Valuable information on the ion-induced order-disorder transition can be gained by studying the TE dynamics, which is highly sensitive to intra- and/or interchain order. For this reason intensity-dependent and frequency-resolved measurements of the PPP-R10/LiOTf blends were carried out, allowing one to study the alterations of TE generation rates, the TE lifetimes, and the bimolecular annihilation parameter which is correlated with the TE diffusion constant.[23] Figure 9 illustrates the evolution of (a) the SE-TE quantum yield

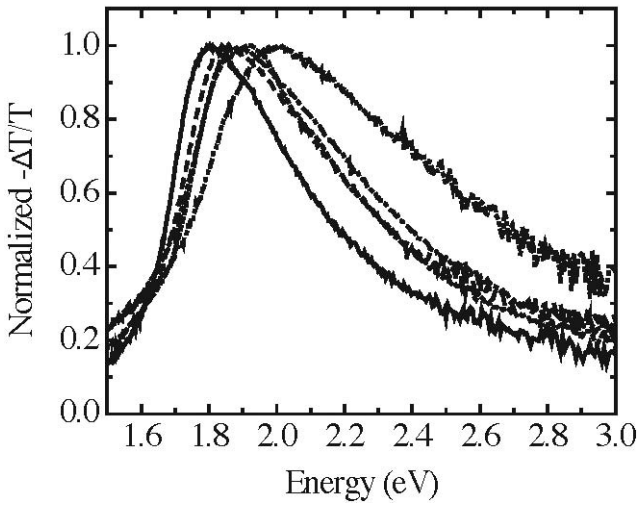

FIG. 8. PIA spectra of thin films of PPP-R10/LiOTf blends. (Solid line) pristine PPP-R10, (dashed line) PPP-R10:LiOTf =20:4 by weight, (short dashed line) PPP-R10:LiOTf=20:6 by weight, (dashed-dotted line) PPP-R10:LiOTf=20:8 by weight, (dashed-dotted-dotted line) PPP-R10:LiOTf=20:16 by weight.

$\eta_{SE\rightarrow TE}$, (b) the monomolecular and the equivalent bimolecular TE lifetimes, $\tau_{TE,mono}$ and $\tau_{TE,bi}$, and (c) the bimolecular annihilation parameter γ_{TE} of pristine and blended PPP-R10.

Figure 9(a) shows the evolution of the TE quantum yield $\eta_{SE\rightarrow TE}$ of pristine PPP-R10 and its LiOTf blended state (maximum concentration polymer to LiOTf 20:16 by weight). Distinctly, an enhancement of the conversion rate from SE to TE with increasing salt content via ISC is detectable. As discussed above, increasing the salt increases the disorder in the complete system, which can be associated with an augmentation of the twist angle between adjacent phenyl rings of the polymer backbone. In case of polythiophenes, Theander *et al.*[39] and Lanzani *et al.*[40] have shown that the fluorescence quantum yield in solution decreases when grafting the polymers with bulky side chains because of more efficient nonradiative decay channels as a consequence of backbone distortion and reduction of π-conjugation. In combination with theoretical studies on different types of π-conjugated oligomers in Ref. 15, which show that an enlargement of the twist angle between adjacent aromatic rings disturbs the π-conjugation of the system and results in to a higher SE-TE conversion yield, we ascribe the rising TE quantum yield with increasing salt concentration to an enhanced SOC in the excited state because of an increasingly nonplanar conformation of the polymer backbones. In other words, the higher TE generation yield of the LiOTf blends arises from more efficient ISC channels involving a nonplanar singlet S_1 excited state and a closer lying triplet state compared to the noncomplexed polymer.[32] For this reason molecular disorder appears to an important parameter in the control of the nonradiative decay rates and the singlet emission quantum efficiencies.

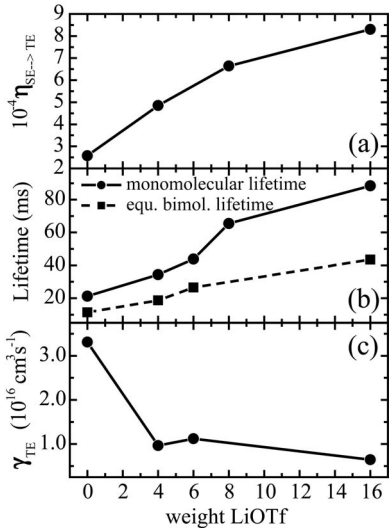

FIG. 9. Evolution of the TE quantum yield (a), TE lifetime (b), and bimolecular annihilation parameter (c) with increasing LiOTf concentration in PPP-R10/LiOTf blend systems.

In Fig. 9(b) the dependence of the monomolecular and the equivalent bimolecular TE lifetime in pristine PPP-R10 and the polymer blended with different concentrations of LiOTf (at comparable excitation densities) are displayed. Both lifetimes increase with increasing lithium salt concentration. In the monomolecular case $\tau_{TE,mono}$ was determined to be 21 ms for the pristine polymer and 88 ms for the blend with the highest LiOTf concentration (20:16), whereas in the bimolecular instance $\tau_{eq,bi}$ increases from 11 ms for the pristine polymer to 43 ms for the 20:16 blend.

Due to the polar side chains and the relatively nonpolar conjugated backbone, films of pristine PPP-R10 were found to reveal highly ordered main chains incorporated into a crystalline side-chain matrix.[31] Such a highly ordered structure will result in relatively low lifetimes, since on-chain as well as interchain migration of TEs is possible and therefore a high manifold of defects, which act as quenching centers, both on the same chain and on neighbored chains can be easily reached. Blending the polymer with LiOTf induces disorder in the main chains, yielding higher twist angles between neighboring phenyl rings. Hence, the intermolecular distance between the conjugated backbones will increase and the interchain migration of TEs is suppressed, i.e., mainly on-chain defects can act as quenching sites and therefore the monomolecular lifetime of the TEs in these systems increases.

It has to be noted that Lauter *et al.*[31] mainly observed a "one-dimensional swelling" upon complexation with LiOTf (in direction of the side-chain matrix). However, their study was performed for a Li:O ratio of 0.04, while the ratios studied here are much higher. A PPP-R10:LiOTf ratio of 20:4, which indeed causes a pronounced influence within the x-ray spectra, but only a small shift within the photophysical characteristics (for which the conjugated backbone moiety is responsible) corresponds to a Li:O ratio of about 0.1. This means that a larger number of ionic species are necessary for a measurable influence on the intermolecular distances of the PPP backbones.

Figure 9(c) depicts the bimolecular annihilation parameter γ_{TE} of a pristine PPP-R10 film and for blends with different concentrations of LiOTf. γ_{TE} is calculated from $\tau_{eq,bi}$ for a given TE density as described in the appendix in detail.

The bimolecular annihilation parameter decreases from 3.3×10^{-16} cm^3 s^{-1} in the pristine polymer to 6.5×10^{-17} cm^3 s^{-1} in the 20:16 blend. Note that the TE diffusion constant is directly related to the annihilation parameter, meaning that the overall mobility of the triplets decreases with increasing LiOTf concentration. This trend is confirmed by quantum mechanical calculations[32] on isolated PPP-R10 backbones (interchain migration of TE is not possible). This shows that on-chain migration and energy transfer of TEs is the more hindered the higher the twisting angles between adjacent phenyl rings (introduced here by the addition of LiOTf), which additionally results in higher lifetimes, since TEs hardly meet on-chain quenching sites.

IV. CONCLUSION

We have shown that the addition of the alkali metal salt LiOTf to oligoether functionalized PPP-type polymers introduces disorder in the systems, resulting in a hypsochromic shift when studying the optical characteristics in the singlet exciton manifold including photoluminescence emission and π-π^* absorption. Additionally, the FWHM of the absorption peaks reveal a strong broadening with high LiOTf concentrations. The introduction of disorder by the addition of the alkali metal salt results in a phase transition from a lamellar-type ordered structure to a random amorphous phase, as confirmed by x-ray measurements.

From PIA measurements on pristine PPP-R10, PPP-OR11, and PPP-R10/OR11 samples, it was found that the more twisted the polymer backbones, the energetically higher is the TE absorption peak located. This conclusion is confirmed by a comparison of the TE absorption maxima of the polymers with that of planar PPP-type polymers (PFO and m-LPPP).

Analyzing the TE absorption features of the pristine polymers and their LiOTf blended state (ratio 20:4 by weight), a similarity concerning the energetic shift as well as the broadening of the TE absorption peak with the π-π^* absorption becomes evident. From the PIA measurements we additionally conclude that an increasing salt concentration result in an enhancement of the ISC rate of singlet excitons to the triplet manifold. This is a consequence of an enhanced SOC because of more nonplanar conformations of the polymer backbones. Additionally, the lifetime of the TEs increases and the TE bimolecular annihilation parameter, which is correlated with the diffusion constant, decreases with the LiOTf ratio. The former behavior can be explained by an increase of the intermolecular distance between adjacent conjugated backbones; thus, interchain migration of TEs is suppressed and mainly on-chain defects act as quenching sites, while the latter characteristic is in accordance with quantum-mechanical calculations.

ACKNOWLEDGMENTS

This work was partially supported by a grant from the AFOSR (FA955-06-1-0192) at the University of Florida. The CDL-AFM gratefully acknowledges the continuous support of AT&S AG.

APPENDIX

Upon photoexcitation only SEs are generated in conjugated polymers. The created SEs can decay radiatively by emitting photons or nonradiatively by emitting phonons, creating polarons due to dissociation (e.g., by chemical defects[36] or an electrical field[41]) or TEs via ISC. ISC is an essential effect for molecules containing heavy atoms, because then spin-orbit coupling become large. The density of TEs depends on the absorbed photons on a unit cross-sectional area of the sample per second N_{abs} and the conversion quantum yield of SEs to TEs $\eta_{\mathrm{SE}\rightarrow\mathrm{TE}}$. For TEs there exist two different recombination regimes: first, the monomolecular decay regime for low TE densities and second, the bimolecular recombination regime, which is observed for high TE densities.

1. Monomolecular regime

The monomolecular decay dynamic is characterized by a linear dependence of the TE population on N_{abs}. This regime is also noticed in systems where polymer chains are isolated from each other, such as in solutions.[42]

The rate equation for the monomolecular decay kinetics of the TEs is given by

$$\frac{dn_{\mathrm{TE,mono}}}{dt}=\eta_{\mathrm{SE}\rightarrow\mathrm{TE}}\times N_{\mathrm{abs}}-k_{\mathrm{TE}}\times n_{\mathrm{TE,mono}}, \quad \text{(A1)}$$

where $\eta_{\mathrm{TE}\rightarrow\mathrm{SE}}$ is the TE quantum yield and $\eta_{\mathrm{SE}\rightarrow\mathrm{TE}}\times N_{\mathrm{abs}}$ the formation rate of TEs from SEs, k_{TE} is the monomolecular TE decay rate, and $n_{\mathrm{TE,mono}}$ is the abbreviation for the TE density in the monomolecular case.

2. Bimolecular regime

The bimolecular TE recombination, which leads to a sublinear dependence of the TE population on N_{abs}, is obtained due to additional TE decay resulting from TE-TE interactions. This recombination kinetic depends on the density of the TEs and its interaction strength.

In order to describe the TE kinetics for both the monomolecular and the bimolecular TE decay region, a further term has to be added to Eq. (A1). One obtains

$$\frac{dn_{\mathrm{TE}}}{dt}=\eta_{\mathrm{SE}\rightarrow\mathrm{TE}}\times N_{\mathrm{abs}}-k_{\mathrm{TE}}\times n_{\mathrm{TE}}-\gamma_{\mathrm{TE}}\times n_{\mathrm{TE}}{}^2, \quad \text{(A2)}$$

containing $-\gamma_{\mathrm{TE}}\times n_{\mathrm{TE}}{}^2$, which describing the bimolecular TE recombination process. γ_{TE} is the bimolecular annihilation parameter. The bimolecular annihilation parameter γ_{TE} is a measure for the TE diffusion. The TE diffusion coefficient D_{TE} can be calculated by

$$D_{\mathrm{TE}}=\frac{\gamma_{\mathrm{TE}}}{4\times\pi\times R}[\mathrm{cm}^2\mathrm{s}^{-1}]. \quad \text{(A3)}$$

R is the extent of the TE wave function. In Ref. 36, the extent of TEs in m-LPPP, which is similar to the here used PPPs, was determined to a value of 3–4 Å.

3. Frequency-resolved PIA measurements

In order to study the TE kinetics concerning their lifetime in the monomolecular and the bimolecular instances,

frequency-resolved PIA measurements were performed. Its principle is to detect the out-of-phase component of the PIA signal as a function of the excitation frequency, given by the chopper, at a fixed wavelength (maximum of the triplet absorption peak) to deduce the time constants of the process.

In the monomolecular case, the frequency $f_{\mathrm{max,mono}}$ at the maximum of the out-of-phase component is related to the monomolecular TE decay rate k_{TE} as shown in the following equation:[43]

$$k_{\mathrm{TE}} = 2\pi \times f_{\mathrm{max,mono}}[\mathrm{s}^{-1}]. \tag{A4}$$

The TE lifetime τ_{TE} in the monomolecular case is the reciprocal of the monomolecular decay rate k_{TE},

$$\tau_{\mathrm{TE}} = \frac{1}{k_{\mathrm{TE}}}[\mathrm{s}]. \tag{A5}$$

The bimolecular recombination process is described by the term $-\gamma_{\mathrm{TE}} \times {n_{\mathrm{TE}}}^2$ in the rate Eq. (A2). This term can be rewritten into the form $-\gamma_{\mathrm{TE}} \times {n_{\mathrm{TE}}}^2 = -(\gamma_{\mathrm{TE}} \times n_{\mathrm{TE}}) \times n_{\mathrm{TE}}$, achieving the equivalent-bimolecular decay rate $k_{\mathrm{eq,bi}}$,

$$k_{\mathrm{eq,bi}} = \gamma_{\mathrm{TE}} \times n_{\mathrm{TE,bi}}[\mathrm{s}^{-1}], \tag{A6}$$

which can be determined from the frequency $f_{\mathrm{max,bi}}$ where the out-of-phase component of the PIA signal exhibits its maximum. The equivalent bimolecular decay rate can be calculated via the following equation:

$$k_{\mathrm{eq,bi}} = 2\pi \times f_{\mathrm{max,bi}}, \tag{A7}$$

and similar to the monomolecular case the equivalent bimolecular TE lifetime $\tau_{\mathrm{TE,bi}}$ is the reciprocal of the equivalent bimolecular decay rate $k_{\mathrm{eq,bi}}$,

$$\tau_{\mathrm{TE,bi}} = \frac{1}{k_{\mathrm{eq,bi}}}[\mathrm{s}]. \tag{A8}$$

4. Intensity-dependent PIA measurements

In order to calculate the quantum yield for SE-TE conversion $\eta_{\mathrm{SE}\rightarrow\mathrm{TE}}$ and the bimolecular annihilations parameter γ_{TE}, the TE density n_{TE} at certain excitation intensities in the monomolecular recombination and the bimolecular recombination regime are required. In principle, the PIA signal $\Delta T/T$ as a function of the excitation intensity and laser power, respectively, at a fixed wavelength (maximum of the triplet absorption peak) is detected, and by using the following equation the TE density can be calculated:

$$n_{\mathrm{TE}} = \frac{\Delta T}{T} \times \frac{1}{\sigma_{\mathrm{TT}} d}[\mathrm{cm}^{-3}]. \tag{A9}$$

$\Delta T/T$ is the PIA signal for the adjusted excitation density, $\sigma_{\mathrm{TT}} \approx 4 \times 10^{-16}$ cm^2 is the absorption cross section of the TEs,[44] and d is the film thickness.

5. TE quantum yield $\eta_{\mathrm{SE}\rightarrow\mathrm{TE}}$ and bimolecular annihilation parameter γ_{TE}

With the results obtained from the frequency-resolved and the intensity-dependent PIA measurements, the TE quantum yield $\eta_{\mathrm{SE}\rightarrow\mathrm{TE}}$ and the bimolecular annihilation parameter γ_{TE} can be calculated. In order to determine $\eta_{\mathrm{SE}\rightarrow\mathrm{TE}}$, we consider the monomolecular steady state rate equation

$$\frac{dn_{\mathrm{TE,mono}}}{dt} = \eta_{\mathrm{SE}\rightarrow\mathrm{TE}} \times N_{\mathrm{abs}} - k_{\mathrm{TE}} \times n_{\mathrm{TE,mono}} = 0. \tag{A10}$$

Thus the TE quantum yield is given by

$$\eta_{\mathrm{SE}\rightarrow\mathrm{TE}} = \frac{k_{\mathrm{TE}} \times n_{\mathrm{TE,mono}}}{N_{\mathrm{abs}}}[-]. \tag{A11}$$

The bimolecular annihilation parameter is given by Eq. (A6) and we obtain

$$\gamma_{\mathrm{TE}} = \frac{k_{\mathrm{eq,bi}}}{n_{\mathrm{TE,bi}}}[\mathrm{s}^{-1}\ \mathrm{cm}^{-3}]. \tag{A12}$$

*Corresponding author. Electronic mail: e.list@tugraz.at

[1] J. H. Burroughes, D. D. C. Bradley, A. R. Brown, R. N. Marks, K. Mackay, R. H. Friend, P. L. Burn, and A. B. Holmes, Nature **347**, 539 (1990).
[2] Q. Pei and Y. Yang, J. Am. Chem. Soc. **118**, 7416 (1996).
[3] R. H. Friend, R. W. Gymer, A. B. Holmes, J. H. Burroughes, R. N. Marks, C. Taliani, D. D. C. Bradley, D. A. Dos Santos, J. L. Brédas, M. Lögdlund, and W. R. Salaneck, Nature **397**, 121 (1999).
[4] M. Aldissi, J. Power Sources **94**, 219 (2001).
[5] D. T. McQuade, A. E. Pullen, and T. M. Swager, Chem. Rev. (Washington, D.C.) **100**, 2537 (2000).
[6] L. Holzer, B. Winkler, F. P. Wenzl, S. Tasch, L. Dai, A. W. H. Mau, and G. Leising, Appl. Phys. Lett. **75**, 2014 (1999).
[7] S. P. Speakman, G. G. Rozenberg, K. J. Clay, W. I. Milne, A. Ille, I. A. Gardner, E. Bresler, and J. H. G. Steinke, Org. Electron. **2**, 65 (2001).
[8] I. Riess, Solid State Ionics **136&137**, 1119 (2000).
[9] U. Lauter, W. H. Meyer, and G. Wegner, Macromolecules **30**, 2092 (1997).
[10] Q. Pei, G. Yu, C. Zhang, Y. Yang, and A. J. Heeger, Science **269**, 1086 (1995).
[11] Q. Pei, Y. Yang, G. Yu, C. Zhang, and A. J. Heeger, J. Am. Chem. Soc. **118**, 3922 (1996).
[12] P. G. Bruce and C. A. Vincent, J. Chem. Soc., Faraday Trans. **89**, 3187 (1993).
[13] F. P. Wenzl, P. Pachler, C. Suess, A. Haase, P. Poelt, E. J. W. List, D. Somitsch, P. Knoll, U. Scherf, and G. Leising, Adv. Funct. Mater. **14**, 441 (2004).
[14] F. Habrard, T. Ouisse, O. Stephan, M. Armand, M. Stark, S. Huant, E. Dubard, and J. Chevrier, J. Appl. Phys. **96**, 7219 (2004).
[15] D. Beljonne, Z. Shuai, G. Pourtois, and J. L. Brédas, J. Phys. Chem. A **105**, 3899 (2001).

[16] M. Wohlgenannt, K. Tandon, S. Mazumdar, S. Ramasesha, and Z. V. Vardeny, Nature **409**, 494 (2001).
[17] Z. Shuai, D. Beljonne, R. J. Silbey, and J. L. Brédas, Phys. Rev. Lett. **84**, 131 (2000).
[18] M. Reufer, M. J. Walter, P. G. Lagoudakis, A. B. Hummel, J. S. Kolb, H. G. Roskos, U. Scherf, and J. M. Lupton, Nat. Mater. **4**, 340 (2005).
[19] G. Mauthner, M. Collon, F. P. Wenzl, M. Bouguettaya, J. R. Reynolds, and E. J. W. List, J. Appl. Phys. **97**, 063508 (2005).
[20] T. Piok, H. Plank, G. Mauthner, S. Gamerith, C. Gadermaier, F. P. Wenzl, S. Patil, R. Montenegro, M. Bouguettaya, J. R. Reynolds, U. Scherf, K. Landfester, and E. J. W. List, Jpn. J. Appl. Phys., Part 1 **44**, 479 (2005).
[21] P. Balanda, Ph.D. thesis, University of Florida, 1997.
[22] G. Heimel, M. Daghofer, J. Gierschner, E. J. W. List, A. C. Grimsdale, K. Müllen, D. Beljonne, J. L. Brédas, and E. Zojer, J. Chem. Phys. **122**, 54501 (2005).
[23] M. Pope and C. A. Swenberg, *Electronic Processes in Organic Crystals*, 2nd ed. (Oxford University Press, New York, 1999).
[24] J. Cornil, D. Beljonne, R. H. Friend, and J. L. Brédas, Chem. Phys. Lett. **223**, 82 (1994).
[25] F. Meyers, A. J. Heeger, and J. L. Brédas, J. Chem. Phys. **97**, 2750 (1992).
[26] E. J. W. List, C. Creely, G. Leising, N. Schulte, A.-D. Schlüter, U. Scherf, K. Müllen, and W. Graupner, Chem. Phys. Lett. **325**, 132 (2000).
[27] R. C. McCullough, Adv. Mater. (Weinheim, Ger.) **10**, 93 (1998).
[28] L. Holzer, B. Winkler, S. Tasch, L. Dai, A. Mau, and G. Leising, Synth. Met. **100**, 71 (1999).
[29] F. P. Wenzl, L. Holzer, S. Tasch, U. Scherf, K. Müllen, B. Winkler, A. Mau, L. Dai, and G. Leising, Synth. Met. **102**, 1138 (1999).
[30] F. P. Wenzl, G. Mauthner, M. Collon, E. J. W. List, C. Suess, A. Haase, G. Jacobic, D. Somitsch, P. Knoll, M. Bouguettaya, J. R. Reynolds, and G. Leising, Thin Solid Films **433**, 287 (2003).
[31] U. Lauter, W. H. Meyer, V. Enkelmann, and G. Wegner, Macromol. Chem. Phys. **199**, 2129 (1998).
[32] H. Wiesenhofer, Ph.D. thesis, Graz University of Technology, 2005.
[33] M. Wohlgenannt and Z. Vardeny, Synth. Met. **125**, 55 (2002).
[34] K. Petritsch, W. Graupner, G. Leising, and U. Scherf, Synth. Met. **84**, 625 (1997).
[35] E. J. W. List, C.-H. Kim, A. K. Naik, U. Scherf, G. Leising, W. Graupner, and J. Shinar, Phys. Rev. B **64**, 155204 (2001).
[36] E. J. W. List, J. Partee, J. Shinar, U. Scherf, K. Müllen, E. Zojer, K. Petritsch, G. Leising, and W. Graupner, Phys. Rev. B **61**, 10807 (2000).
[37] T. Piok and E. J. W. List (unpublished).
[38] M. A. Loi, C. Gadermaier, E. J. W. List, G. Leising, W. Graupner, G. Bongiovanni, A. Mura, J.-J. Pireaux, and K. Kaeriyama, Phys. Rev. B **61**, 1859 (2000).
[39] M. Theander, O. Inganas, W. Mammo, T. Olinga, M. Svensson, and M. R. Andersson, J. Phys. Chem. B **103**, 7771 (1999).
[40] G. Lanzani, M. Noisoli, and R. Tubino, Synth. Met. **76**, 39 (1996).
[41] B. Schweitzer, V. I. Arkhipov, U. Scherf, and H. Bässler, Chem. Phys. Lett. **313**, 57 (1999).
[42] R. Janssen, N. Sariciftci, K. Pakbaz, J. McNamara, S. Schricker, A. J. Heeger, and F. Wudl, Synth. Met. **69**, 441 (1995).
[43] V. Dyakonov, G. Rösler, M. Schwoerer, and E. L. Frankevich, Phys. Rev. B **56**, 3852 (1997).
[44] A. P. Monkman, H. D. Burrows, M. G. Miguel, I. Hamblett, and S. Navaratnam, Chem. Phys. Lett. **307**, 303 (1999).